Evaluation of the Effects of Injection Velocity and Different Gel Concentrations on Nanoparticles in Hyperthermia Therapy

Javidi M[1,2], Heydari M[1,2], Karimi A[1,2], Haghpanahi M[1], Navidbakhsh M[1,2*], Razmkon A[3]

[1]School of Mechanical Engineering, Iran University of Science and Technology, Tehran 16846, Iran
[2]Tissue Engineering and Biological Systems Research Laboratory, School of Mechanical Engineering, Iran University of Science and Technology, Tehran 16846, Iran
[3]Department of Neurosurgery, Shiraz University of Medical Sciences, Shiraz, Iran

ABSTRACT

Background and objective: In magnetic fluid hyperthermia therapy, controlling temperature elevation and optimizing heat generation is an immense challenge in practice. The resultant heating configuration by magnetic fluid in the tumor is closely related to the dispersion of particles, frequency and intensity of magnetic field, and biological tissue properties.

Methods: In this study, to solve heat transfer equation, we used COMSOL Multiphysics and to verify the model, an experimental setup has been used. To show the accuracy of the model, simulations have been compared with experimental results. In the second part, by using experimental results of nanoparticles distribution inside Agarose gel according to various gel concentration, 0.5%, 1%, 2%, and 4%, as well as the injection velocity, 4 $\mu L/min$, 10 $\mu L/min$, 20 $\mu L/min$, and 40 $\mu L/min$, for 0.3 cc magnetite fluid, power dissipation inside gel has been calculated and used for temperature prediction inside of the gel.

Results: The Outcomes demonstrated that by increasing the flow rate injection at determined concentrations, mean temperature drops. In addition, 2% concentration has a higher mean temperature than semi spherical nanoparticles distribution.

Conclusion: The results may have implications for treatment of the tumor and any kind of cancer diseases.

Keywords

Hyperthermia, Bio-heat transfer equation, Magnetic fluid, Nanoparticles distribution, Power dissipation

Introduction

Body temperature is elevated in hyperthermia due to failed thermoregulation that occurs when a body produces or absorbs more heat than it dissipates. Extreme temperature elevation becomes a medical emergency requiring immediate treatment to prevent disability or death. It can also be deliberately induced using drugs or medical devices and may be used in the treatment of some kinds of cancer and other conditions, most commonly in conjunction with radiotherapy. Hyperthermia uses physical methods to heat determined tissues to the temperatures in the range of 40–46 °C with treatment time approximately one hour [1-3].

Research has shown that high temperatures can damage and kill cancer cells, usually with minimal injury to normal tissues. It is proposed that by

*Corresponding author:
M Navidbakhsh
School of Mechanical Engineering, Iran University of Science and Technology, Tehran 16846, Iran
E-mail: mnavid@iust.ac.ir

killing cancer cells and damaging proteins and structures within the cells, hyperthermia may shrink tumors to make the cells more sensitive to radiation therapy (RT) and chemotherapy [4]. In some cases, if the elevated temperature is utilized as the stand alone technique, tissue temperature above 48 degrees would be the objective.

Hyperthermia induces almost reversible damage to cells and tissues, but as an adjunct it enhances radiation injury of tumor cells and chemotherapeutic efficacy. Because of the results that high temperature may produce in tissues, one can refer to use of temperatures > 50 $°C$ as coagulation, 60 to 90$°C$ as thermal ablation, > 200 $°C$ as charring [5].

However, MFH is not widely applied in clinical treatments due to the difficulty in the accurate determination of temperature distribution within target tissue, precise control of thermal dose, and uniform heating [6]. Most investigations, as well as clinical applications, have focused on the heating effects and specific absorption rates (SAR) of magnetic fluids [6].

In clinical applications of magnetic fluid hyperthermia for cancer treatment, it is very important to ensure maximum damage to the tumor while protecting the normal tissue. In magnetic fluid hyperthermia, the magnetic nanoparticles are delivered to the tumor. Two techniques are currently used to deliver particles to a tumor. First is to deliver them to the tumor vasculature through its supplying artery; however, this method is not effective for poorly perfused tumors. Moreover, for a tumor with an irregular shape, inadequate particle distribution may cause under-dosage of heating in the tumor or overheating of the normal tissue. The second approach is to directly inject them into the extracellular space in tumors. They diffuse inside the tissue after injection of ferrofluid. If the tumor has an irregular shape, multisite injection can be exploited to cover the entire target region [5].

Experiments on magnetic particle diffusion in Agarose gel and animal tissue were performed to study their migration in gel and to evaluate the local blood perfusion rate and amount of nanofluid delivered to target region by Salloum *et al* [7, 8].

The improvement of mathematical models for heat transfer in living tissues has been a topic of interest for various biologists, physicians, mathematicians and also engineers. The accurate explanation of the thermal interaction between vasculature and tissues is necessary for the encroachment of medical technology in treating fatal diseases such as tumor [2, 9-11].

The Pennes bio-heat transfer equation model has been broadly used among different bio-heat models [12]. This model shows the effect of blood perfusion as a temperature-dependent heat sink term and practically simulate convection heat transfer of blood. It is assumed that the blood perfusion effect is homogeneous and isotropic, and that thermal equilibration occurs in the micro-circulatory capillary bed. Due to the complication of tissues and their complex geometry, exact solutions are not available in many cases [13].

Baish proposed a new model to simulate heat transportation tissue with a tree-like distribution of thermally significant vessels [14]. This model used an algorithm to simulate the geometry of a realistic vascular tree, and solved the conjugate heat transfer problem of convection by the blood coupled to three dimensional conduction in the tissue along the vascular tree [15-17]. For a given application, this model must include a sufficiently detailed representation of the vasculature to predict the temperature field. On the other hand, some researchers have investigated heat transfer in biological tissue by using the theory of porous media to simplify the vascular structure of the tissue [18, 19].

In many practical applications, numerical models such as the finite element method [20, 21], finite difference method [22, 23] and Monte Carlo method [24, 25], lattice Boltzmann method are used [26]. In the most of numerical studies, homogenous nanoparticles dis-

tribution or heat generation inside tumor and healthy tissue have been considered. In similar works, like Dughiero *et al* [27], an automated procedure of optimization is used, based on evolutionary computing and finite element analysis in order to find the position of multiple NPs injections determining a tumor temperature close to the therapeutic value. They assumed spatial function of the NPs concentration with a Gaussian shape and regular geometry of tumor. Pavel *et al* [28] performed a systematical variation of tumor diameter and particle dosage for every physical parameter of above mentioned tumor tissues (e.g., tissue density, tumor/tissue perfusion rate). By this systematization they intended to understand the interdependence of these parameters and their effects on hyperthermia therapy. They considered three models to investigate. The first model designed a cubical region, two blood vessels with a diameter of 0.5 *mm* and 1.2 *mm*, respectively were located at 7.5 *mm* each from the tumor border and tumor was configured as a perfect sphere. In the second model computed, they assumed the presence of one blood vessel more of 2.8 *mm* in diameter, near to the tumor region at 1–2 *mm* distance from it [29-32]. In the third model, they estimated the variation of tumor border temperature when the tumor diameter is varied for different concentration of magnetic material and different loss power. The nanoparticles were randomly concentrated in 6 regions of 0.9 *mm* diameter each inside the tumor area.

In This study, COMSOL Multiphysics was employed to solve heat transfer equation. First, by comparing experimental data with calculated temperature regarding to heat generation inside an agar gel, the numerical procedure is validated.

Particular attention is given to the influence of the collective behaviors of nanoparticles in suspension [33].

Since nanoparticle distribution in tumors is a main factor determining the resulting heating pattern and therapeutic outcome of a magnetic hyperthermia treatment, by using determined nanoparticles distribution proposed by Salloum *et al* [7] and power dissipation equation, we calculated heat generation source in heat transfer equation and abled to find temperature variation inside Agarose gel. The main advantage of this work is using real particles distribution and finding heat generation inside the gel according to several parameters like spatial coordinates, magnetic field frequency and amplitude. It is evident that velocity injection rate, gel concentration effect particles distribution and eventually heat generation distribution.

Methods

In anatomical studies, the vascular structure of a tumor has been found to be different from that of normal tissue [34]; the geometry of the vasculature in tumors is very complicated and quantitative data on this irregular structure is sparse. Therefore, the vascular structures of tumor and normal tissue have been assumed to be the same in order to simplify the physical model. Based on this assumption, the entire domain, including tissue and tumor, is taken to be a cylinder. See figure 1.

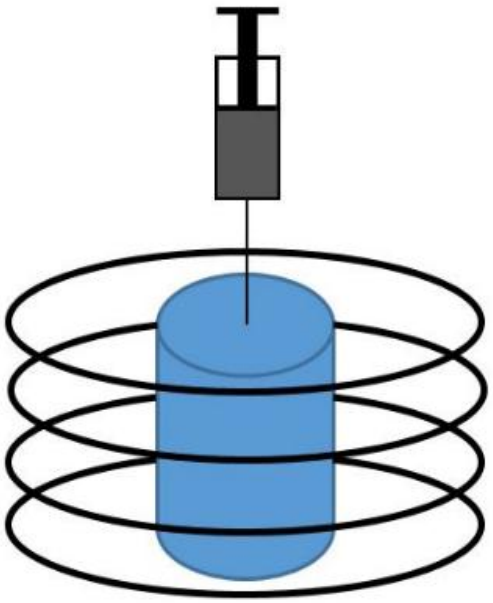

Figure 1: Schematic of coil and sample.

Blood effect has been modeled as an isotropic heat source or sink which is proportional to blood flow rate and the difference between the body core temperature and local tissue temperature by Pennes [12]. Therefore, He suggested a model to describe the effects of metabolism and blood perfusion on the energy balance within tissue. These two effects were incorporated into the standard thermal diffusion equation, which is written in its simplified form as:

$$k\nabla^2 T - w_b \rho_b c_{pb}(T - T_b) + Q_m + Q_s = \rho c_p \frac{\partial T}{\partial t} \quad (1)$$

where ρ, c_p and k are the density, the specific heat, and the thermal conductivity of the tissue, respectively. T is the temperature, t the time, w_b, ρ_b, c_{bp} and T_b are the perfusion, the density, the specific heat and the temperature of the blood, and Q_m are the metabolic heat generation of the tissue and the Q_s distributed volumetric heat generation due to spatial heating.

Pennes performed a series of experimental studies to validate his model. Validations have shown that the results of Pennes bio-heat model are in a reasonable agreement with the experimental data [12].

It is clear that the distribution of nanoparticles will affect the heat source distribution inside tissue. Hence, considering the particles distribution inside of tissue is essential, for this purpose, we should know about power dissipation of particles for different distributions. The power dissipation of magnetic nanoparticles which are subjected to an alternating magnetic field is expressed as equation 2 [35, 36]:

$$P = \pi \mu_0 x_0 H_0^2 f \frac{2\pi f \tau}{1 + (2\pi f \tau)^2} \quad (2)$$

where $\mu_0 = 4\pi \times 10^{-7}$ $T.m/A$ is the permeability of free space, x_0 is the equilibrium susceptibility, H_0 and f are the amplitude and frequency of the alternating magnetic field and τ is the effective relaxation time, given by equation (3):

$$\tau^{-1} = \tau_N^{-1} + \tau_B^{-1} \quad (3)$$

where τ_N and τ_B are Néel and the Brownian relaxation time, respectively. τ_N and τ_B are calculated as follow, equations ((4) and (5)):

$$\tau_N = \frac{\sqrt{\pi}}{2} \tau_0 \frac{\exp(\Gamma)}{\sqrt{\Gamma}} \quad (4)$$

$$\tau_B = \frac{3\eta V_H}{kT} \quad (5)$$

where, the shorter time constant tends to dominate in determining the effective relaxation time for any given size of particle. τ_0 is the average relaxation time in response to a thermal fluctuation, η is the viscosity of medium, V_H is the hydrodynamic volume of Magnetic nanoparticles. k is the Boltzmann constant, 1.38×10^{-23} JK^{-1}, and T is temperature. Here, $\Gamma = \frac{KV_M}{KT}$ where K is themagnetocrystalline anisotropy constant and V_m is the volume of Magnetic nanoparticles. The Magnetic nanoparticles volume V_M and the hydrodynamic volume including the ligand layer V_H are written as:

$$V_H = \frac{\pi (D + 2\delta)^3}{6} \quad (6)$$

$$V_M = \frac{\pi D^3}{6} \quad (7)$$

where, D is the diameter of magnetic nanoparticles and δ is the ligand layer thickness.

The equilibrium susceptibility x_0 is assumed to be the chord susceptibility corresponding to the Langevin equation ($\frac{M}{M_s} = coth\xi - \frac{1}{\xi}$) and expressed as:

$$x_0 = x_i \frac{3}{\xi}(coth\xi - \frac{1}{\xi}) \quad (8)$$

where, $\xi = \frac{\mu_0 M_d H V_M}{kT}$, $H = H_0 cos(\omega t)$, $\omega = 2\pi f$, $M_s = \phi M_d$ and ϕ is volume fraction of magnetic nanoparticles. Here, M_d and M_s are

the domain and saturation magnetization, respectively. The initial susceptibility is given by:

$$x_i = \frac{\mu_0 \phi M_d^2 V_M}{3kT} \quad (9)$$

The difficulty of visualizing the nanofluid dispersion is one of the challenges in assessing the energy generation induced in animal tissue. Up to this date, gels are basically the only transparent porous materials that are equivalent to animal tissue for in vitro studies despite the fact that gels are homogeneous in comparison to the complicated tumor morphology [7]. In fact, the tumor extracellular space convection/diffusion properties are found to be similar to the Agarose gel [26].

Results and Discussion

Verification

To verify our model in COMSOL, an experimental setup has been used. For this matter 0.3 *cc* of magnetite nanofluid of Fe_3O_4 with 7% concentration was poured in 6.7 *cc* of 1% agar gel solution in 60 °*C* temperature. This procedure was employed to have a uniform disperse medium of nanoparticles inside gel. The solution was loaded into a cylindrical transparent container and cooled further to room temperature (20°*C*) until solidification. A radiofrequency electromagnetic field is applied to the solution. For measuring temperature inside gel, prototype was took out every 120 seconds from inside coils to record temperature at center of the cylinder.

Properties of Fe_3O_4 magnetic nanoparticles, agar gel and magnetic field are listed on table 1. Equation (2) for heat generation inside medium was employed to volumetric heat generation inside gel.

Geometry of whole gel with nanoparticles considered as an axial finite cylinder with D_i=1.4 *cm* radius and *h*=4.5 cm height and container thickness is *t*=1 *mm*. According to unsteady heat transfer, equation (10) and (11) define the transient heat transport inside gel and container.

$$k_1 \frac{1}{r^2}\frac{\partial}{\partial r}\left(r^2 \frac{\partial T_1}{\partial r}\right) - k_1 \frac{\partial}{\partial z}\left(\frac{\partial T_1}{\partial z}\right) + Q_s = (\rho c)_1 \frac{\partial T_1}{\partial t} \quad for \quad 0 < r < R_i \; and \; 0 < z < h \quad (10)$$

$$k_2 \frac{1}{r^2}\frac{\partial}{\partial r}\left(r^2 \frac{\partial T_2}{\partial r}\right) - k_2 \frac{\partial}{\partial z}\left(\frac{\partial T_2}{\partial z}\right) = (\rho c)_2 \frac{\partial T_2}{\partial t} \quad for \quad R_i < r < R_o \; and \; 0 < z < h \quad (11)$$

Table 1: Properties of magnetic field, nanoparticles and agar gel.

Physical Property	Symbol	Value
Frequency	f	164 (kHz)
Amplitude	H_0	1.2 (kAm^{-1})
Magnetocrystalline Anisotropy	K	9 ($kJ\ m^{-3}$)
Saturation Magnetization	M_s	300 (gauss)
Nanoparticles Diameter	D_{np}	8 (nm)
Nanoparticles Heat Capacity	C_{np}	670 J $(kg\ K)^{-1}$

Here, in equations (10) and (11) $R_i = D_i / 2$ and $R_0 = D_i / 2+t$ are gel and container radius, and subscripts 1 and 2 are gel and container, respectively. In this step, the properties of the gel with dispersed nanoparticles are taken as follows [25]: $\rho_{mix} = \phi\rho_{rp} + (1- \phi)\rho_{gel}$, $\rho_{gel} = 1000\ kgm^{-3}$, $k_1 = k_2 = 0.50\ W\ m^{-1}K$, $c_{mix} = \phi c_{gel} + (1- \phi)c_{gel}$, c_{gel}=4180 $J\ (kg\ K)^{-1}$, $T_0 = T_{0,1} = T_{0,2}$=293.15K, and volume fraction, ϕ =0.003. Calculated properties of heat capacity, density and heat conductivity listed in table 2. As was explained, our prototype is a homogenous medium of nanoparticles and agar gel, therefore heat generation inside gel by equation (2) would be $P = 0.11\times10^5\ W/m^3$.

Table 2: Properties of medium contain nanoparticles.

Physical Property	Symbol	Value
Mixture Heat Capacity	c_{mix}	3890.31 ($Jkg^{-1}K^{-1}$)
Mixture Heat Conductivity	k_{mix}	0.566 ($Wm^{-1}k^{-1}$)
Mixture Density	ρ_{mix}	1011.85 ($kg\ m^{-3}$)

The related boundary conditions are:

$$\frac{\partial T_1}{\partial r}(0,t) = 0 \quad (12)$$

$$T_1(R_i, z, t) = T_2(R_o, z, t) \quad (13)$$

$$k_1 \frac{\partial T_1}{\partial r}(R_i, z, t) = k_2 \frac{\partial T_2}{\partial r}(R_i, z, t) \quad (14)$$

$$k_2 \frac{\partial T_2}{\partial r}(R_o, z, t) = h_{air}(T_2 - T_{air}) \quad (15)$$

Here T_{air} = 293.15 K and h_{air} = 10 $Wm^{-2}K^{-1}$. Initial conditions were:

$$T_1(r, z, 0) = T_0 \quad (16)$$

$$T_2(r, z, 0) = T_0 \quad (17)$$

Figure 2 shows temperature versus time inside computational domain inside gel. There are good agreements between both computational method experimental data till 800 seconds, but after that temperature difference with experimental results becomes bigger. According to Golneshan *et al* [25] and Rodrigues *et al* [37] temperature became steady after some time.

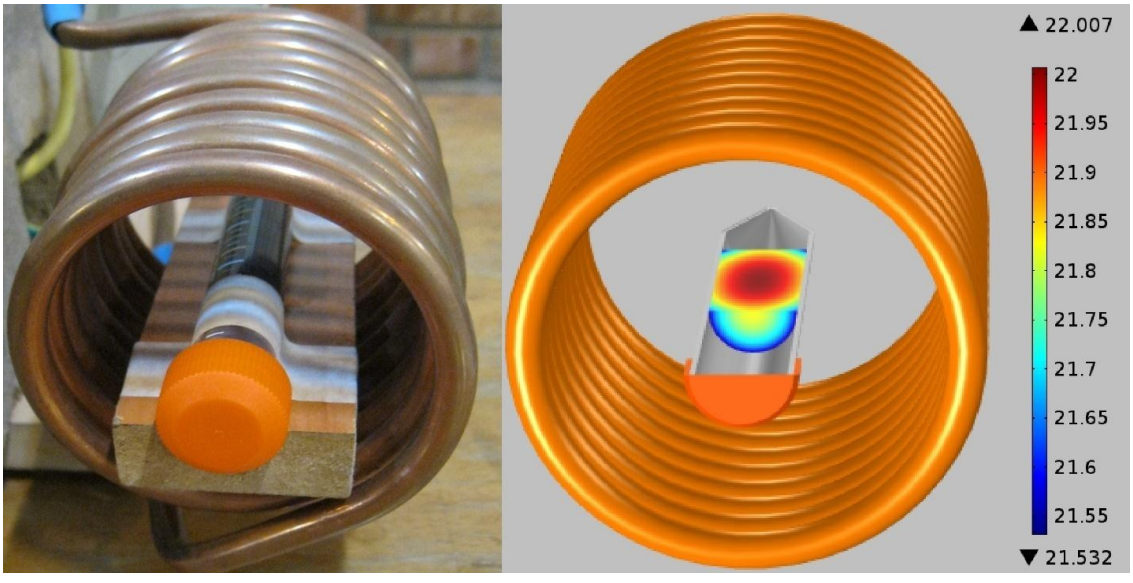

Figure 2: Experimental setup of dispersed nanoparticles inside gel and coils (left), Temperature contours for simulation after 1080 s (right).

Numerical study for different nanoparticles distribution and gel concentration

An axisymmetric assumption for geometry and particles distribution has been made (in figure 3 h=0.05 m, b=0.0125 m, r= 0.0212 m). Figure 4 demonstrates sample tissue and injection site of nanoparticles into the gel. Distributions of the nanoparticles are illustrated in figure 5 for various combination of the gel concentrations and flow rates (from Salloum *et al* [7]). Regarding of distribution of particles, magnetic nanoparticles power dissipation was calculated by equation 2. For this case, the Magnetite nanoparticle properties are as follows: d=10 nm, ρ=5240 kgm^{-3}, c_p = 670 $J(kgK)^{-1}$, ligand layer δ=1 nm, and 0.3 cc ferrofluid solution. For heat generation calculation inside gel we considered a magnetic field with these characteristics: amplitude of alternating magnetic field, H_0=3 kAm^{-1}, frequency of alternating magnetic field, f=325 kHz, dynamic viscosity of medium, η=0.001 Pas, average relaxation time, τ_0=10^{-9} s, domain magnetization M_d=4.46×10^5 kAm^{-1}, anisotropy constant, K=9×10^3 kJm^{-3}.

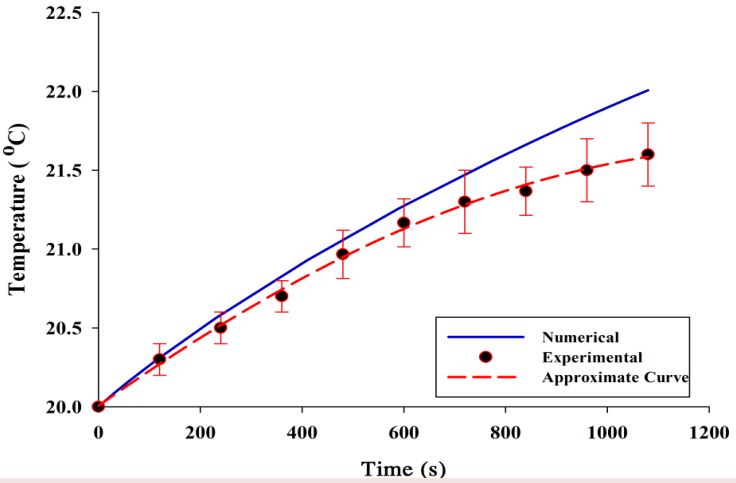

Figure 3: Temperature versus time at center of cylinder.

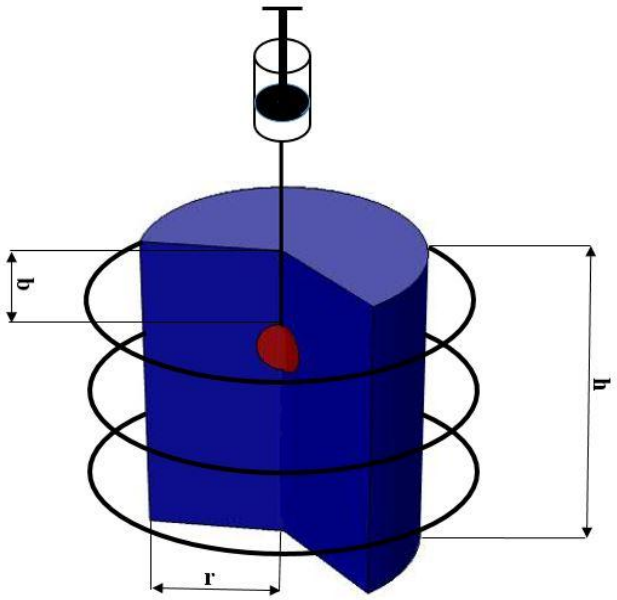

Figure 4: Geometry of considered injection site.

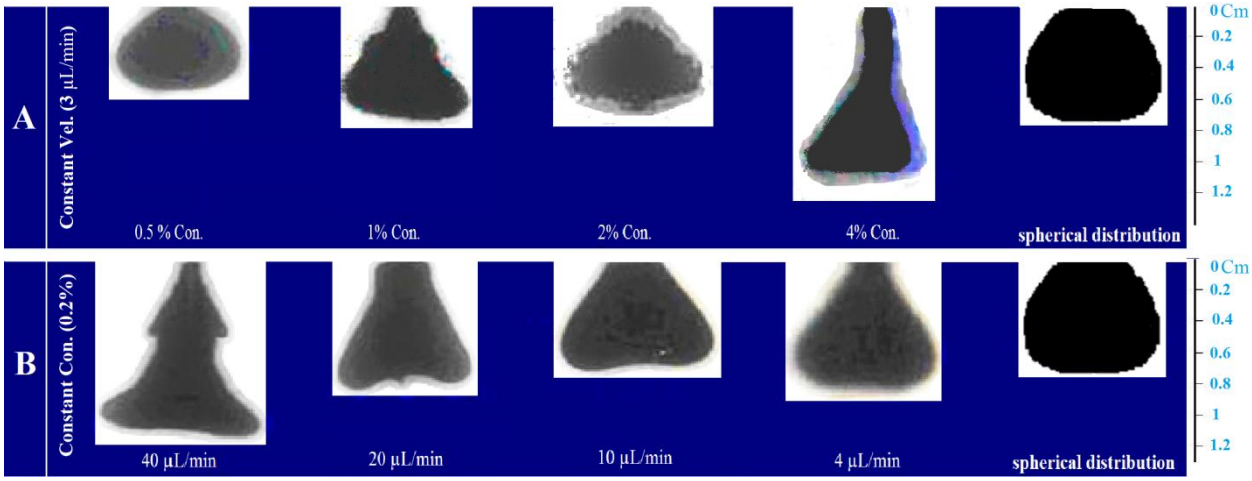

Figure 5: (A) Nanoparticles distribution at different gel concentration with 3 $\mu L / min$ infusion velocity (B) Nanoparticles distribution for different infusion velocity at 0.2% gel concentration.

Figure 6 and figure 7 display variations of temperature along center line. As it has been expected, maximum temperature occurs at the most concentrated areas, and by increasing gel concentration form 0.5% to 2% maximum temperature gets closer to semi spherical maximum value.

To see how injection rate effected temperature trend on the centerline of cylinder, figure 6 has been drawn. By increasing flow rate actually there are no big differences among temperature distribution .However, infusion velocity 4 $\mu L\ min^{-1}$ has a higher maximum temperature in comparison with others.

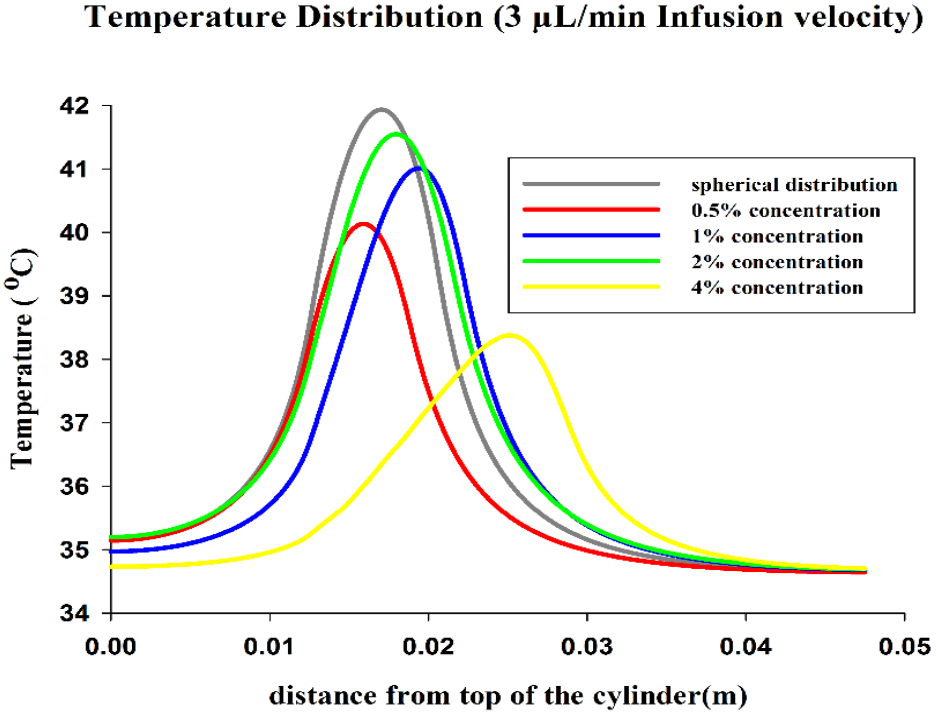

Figure 6: Temperature versus distance from top of the cylinder at centerline for different gel concentration at 3 $\mu L / min$ infusion velocity.

Figures 8 and 9 indicate steady state temperature distribution inside gel at cylinder center line and at the maximum temperature position. As it can be seen from figure 7 with increasing concentration there is no regular pattern. From 0.5% to 2% concentration, mean temperature increases and from 2% to 4% concentration there is a decrement. In comparison to semi spherical distribution, 2% concentration curve has higher temperature in radial direction except region near center line.

Figure 9 displays the temperature distribution versus radius for 0.2% concentration. Spreading with semi spherical shape has upper mean temperature than other forms and its maximum value is 41.91 $^{\circ}C$. Also, by increasing injection rate maximum temperature drops from 41.13 $^{\circ}C$ to 38.37 $^{\circ}C$.

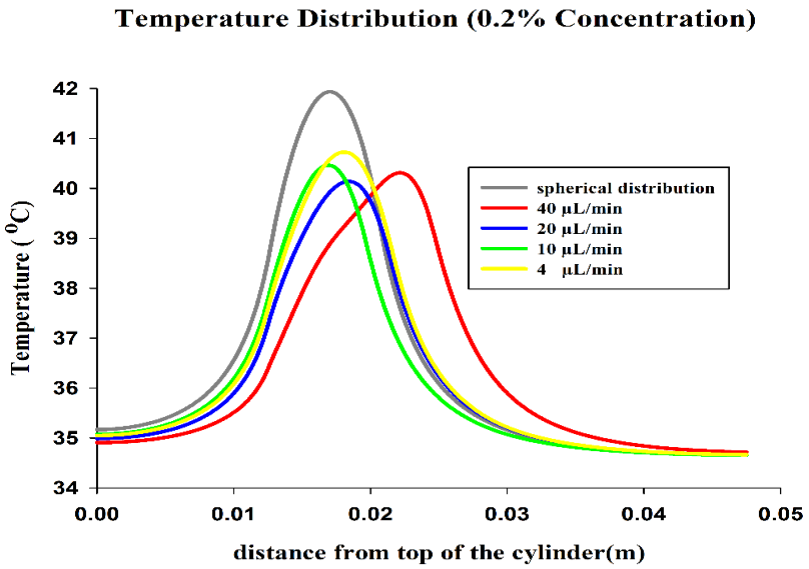

Figure 7: Temperature versus distance from top of the cylinder at centerline for different infusion velocity at 0.2% concentration.

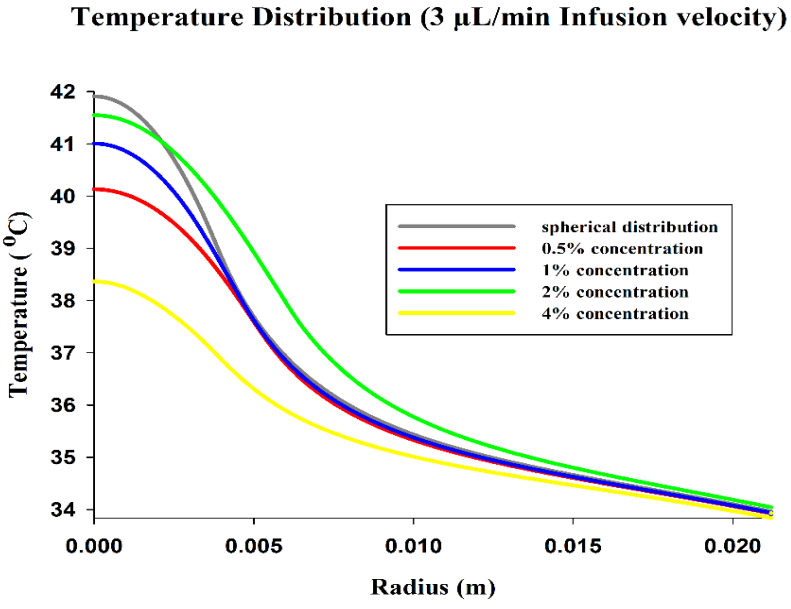

Figure 8: Temperature versus distance from centerline for different gel concentration at 3 μL / *min* infusion velocity.

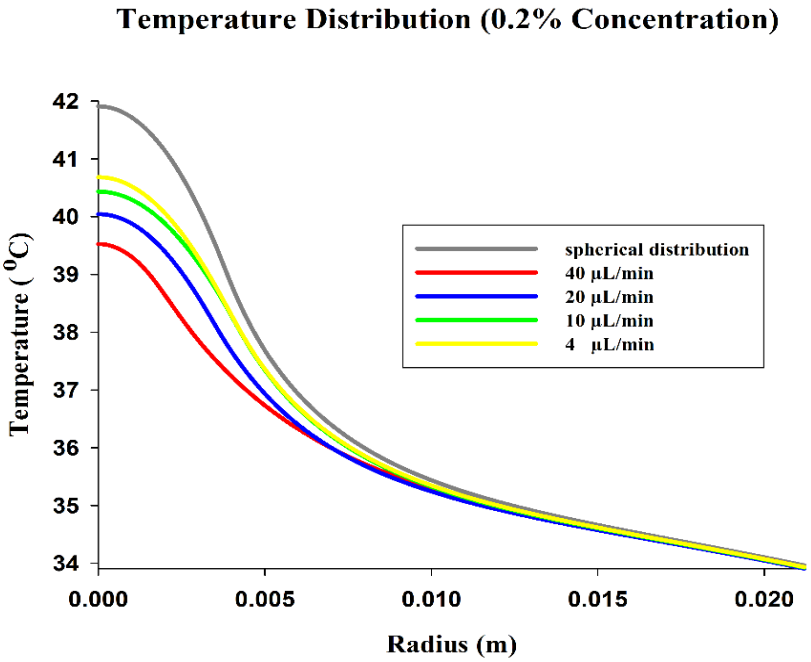

Figure 9: Temperature versus distance from centerline for different infusion velocity at 0.2% concentration.

Conclusion

This study investigated the temperature and the thermal dose response of a biological tissue undergoing hyperthermia therapy, through using experimental results of the infusion flow rate and gel concentration reported by Salloum *et al* [7]. First by assuming exponential heat generation distribution our model has been verified. The results were in good agreement with data stated by Barba *et al* [27]. Moreover, by using experimental results done by Salloum *et al* [4], temperature variation has been plotted for several condition. First because of axisymmetric geometry and physics temperature variation along center line has been displayed and by finding maximum temperature location, temperature distribution along radial direction has been shown.

Conflict of Interest

None

References

1. Habash RW, Bansal R, Krewski D, Alhafid HT. Thermal therapy, part 2: hyperthermia techniques. *Crit Rev Biomed Eng*. 2006;**34**(6):491-542. PMID: 17725480.
2. Gupta PK, Singh J, Rai KN. A numerical study on heat transfer in tissues during hyperthermia. *Math Comput Model*. 2013;**57**(5):1018-37. Doi:10.1016/j.mcm.2011.12.050.
3. Gupta PK, Singh J, Rai KN. Numerical simulation for heat transfer in tissues during thermal therapy. *J Therm Biol*. 2010;**35**(6):295-301. DOI: 10.1016/j.jtherbio.2010.06.007.
4. Byers T, Mouchawar J, Marks J, Cady B, Lins N, Swanson GM, *et al*. The American Cancer Society challenge goals. How far can cancer rates decline in the U.S. by the year 2015? *Cancer*. 1999;**86**(4):715-27. PubMed PMID: 10440701.
5. Chicheł A, Skowronek J, Kubaszewska M, Kanikowski M. Hyperthermia – description of a method and a review of clinical applications. *Rep Pract Oncol Radiother*. 2007;**12**(5):267-75. doi: http://dx.doi.org/10.1016/S1507-1367(10)60065-X.
6. Yue K, Yu C, Lei Q, Luo Y, Zhang X. Numerical simulation of effect of vessel bifurcation on heat transfer in the magnetic fluid hyperthermia. *Appl Therm Eng*. 2014;**69**:11-8. doi: http://dx.doi.org/10.1016/j.applthermaleng.2014.04.035.
7. Salloum M, Ma RH, Weeks D, Zhu L. Controlling nanoparticle delivery in magnetic nanoparticle hyperthermia for cancer treatment: experimental study

in agarose gel. *Int J Hyperthermia*. 2008;**24**(4):337-45. doi: 10.1080/02656730801907937. PubMed PMID: 18465418.

8. Salloum M, Ma R, Zhu L. An in-vivo experimental study of temperature elevations in animal tissue during magnetic nanoparticle hyperthermia. *Int J Hyperthermia*. 2008;**24**(7):589-601. doi: 10.1080/02656730802203377. PubMed PMID: 18979310.
9. Faghihi S, Gheysour M, Karimi A, Salarian R. Fabrication and mechanical characterization of graphene oxide-reinforced poly (acrylic acid)/gelatin composite hydrogels. *J Appl Phys*. 2014;**115**(8):083513-20. DOI: http://dx.doi.org/10.1063/1.4864153.
10. Faghihi S, Karimi A, Jamadi M, Imani R, Salarian R. Graphene oxide/poly(acrylic acid)/gelatin nanocomposite hydrogel: experimental and numerical validation of hyperelastic model. *Mater Sci Eng C Mater Biol Appl*. 2014;**38**:299-305. doi: 10.1016/j.msec.2014.02.015. PubMed PMID: 24656382.
11. Karimi A, Faturechi R, Navidbakhsh M, Hashemi A. A nonlinear hyperelastic behavior to identify the mechanical properties of rat skin under uniaxial loading. *J Mech Med Biol*. 2014;**14**(5):1450075-89. DOI: 10.1142/S0219519414500754.
12. Pennes HH. Analysis of tissue and arterial blood temperatures in the resting human forearm. *J Appl Physiol*. 1998;**85**(1):5-34. PMID: 9714612.
13. Yuan P. Numerical analysis of temperature and thermal dose response of biological tissues to thermal non-equilibrium during hyperthermia therapy. *Med Eng Phys*. 2008;**30**(2):135-43. Doi:10.1016/j.medengphy.2007.03.006.
14. Baish J. Formulation of a statistical model of heat transfer in perfused tissue. *J Biomech Eng*. 1994;**116**(4):521-7. Doi:10.1115/1.2895804. PMID: 7869729.
15. Karimi A, Navidbakhsh M, Razaghi R. A finite element study of balloon expandable stent for plaque and arterial wall vulnerability assessment. *J Appl Phys*. 2014;**116**(5): 044701-10. DOI: http://dx.doi.org/10.1063/1.4891019.
16. Karimi A, Navidbakhsh M, Razaghi R. Plaque and arterial vulnerability investigation in a three-layer atherosclerotic human coronary artery using computational fluid-structure interaction method. *J Appl Phys*. 2014;**116**(9):064701-10. DOI: http://dx.doi.org/10.1063/1.4893368.
17. Karimi A, Navidbakhsh M, Razaghi R, Haghpanahi M. A computational fluid-structure interaction model for plaque vulnerability assessment in atherosclerotic human coronary arteries. *J Appl Phys*. 2014;**115**(14):144702-11. DOI: http://dx.doi.org/10.1063/1.4870945.
18. Shrivastava D, Roemer RB. Readdressing the issue of thermally significant blood vessels using a countercurrent vessel network. *J Biomech Eng*. 2006;**128**(2):210-6. doi: 10.1115/1.2165693. PubMed PMID: 16524332.
19. Khaled ARA, Vafai K. The role of porous media in modeling flow and heat transfer in biological tissues. *Int J Heat Mass Transf*. 2003;**46**(26):4989-5003. doi: http://dx.doi.org/10.1016/S0017-9310(03)00301-6.
20. Emery AF, Sekins KM. The use of heat transfer principles in designing optimal diathermy and cancer treatment modalities. *Int J Heat Mass Transf*. 1982;**25**(6):823-34. doi: http://dx.doi.org/10.1016/0017-9310(82)90095-3.
21. Trakic A, Liu F, Crozier S. Transient temperature rise in a mouse due to low-frequency regional hyperthermia. *Phys Med Biol*. 2006;**51**(7):1673-91. doi: 10.1088/0031-9155/51/7/003. PubMed PMID: 16552097.
22. Samaras T, Christ A, Kuster N. Effects of geometry discretization aspects on the numerical solution of the bioheat transfer equation with the FDTD technique. *Phys Med Biol*. 2006;**51**(11):N221-9. doi: 10.1088/0031-9155/51/11/n02. PubMed PMID: 16723759.
23. Rossi MR, Rabin Y. Experimental verification of numerical simulations of cryosurgery with application to computerized planning. *Phys Med Biol*. 2007;**52**(15):4553-67. doi: 10.1088/0031-9155/52/15/013. PubMed PMID: 17634650; PubMed Central PMCID: PMC2259025.
24. Deng ZS, Liu J. Mathematical modeling of temperature mapping over skin surface and its implementation in thermal disease diagnostics. *Comput Biol Med*. 2004;**34**(6):495-521. doi: 10.1016/s0010-4825(03)00086-6. PubMed PMID: 15265721.
25. Golneshan AA, Lahonian M. Effect of heated region on temperature distribution within tissue during magnetic fluid hyperthermia using lattice Boltzmann method. *J Mech Med Biol*. 2011;**11**(02):457-69. DOI: 10.1142/S0219519410003824.
26. Lahonian M, Golneshan AA. Numerical study of temperature distribution in a spherical tissue in magnetic fluid hyperthermia using lattice Boltzmann method. *IEEE Trans Nano-Bioscience*. 2011;**10**(4):262-8. Doi: 10.1109/TNB.2011.2177100. PubMed PMID: 22271797.
27. Johannsen M, Gneveckow U, Eckelt L, Feussner A, Waldofner N, Scholz R, *et al*. Clinical hyperthermia of prostate cancer using magnetic nanoparticles: presentation of a new interstitial technique. *Int J*

Hyperthermia. 2005;**21**(7):637-47. PubMed PMID: 16304715.

28. Pavel M, Stancu A. Ferromagnetic nanoparticles dose based on tumor size in magnetic fluid hyperthermia cancer therapy. *IEEE Trans Magn*. 2009;**45**(11):5251-4. Doi:10.1109/TMAG.2009.2031076.
29. Abdi M, Karimi A. A Computational Electrical Analogy Model to Evaluate the Effect of Internal Carotid Artery Stenosis on Circle of Willis Efferent Arteries Pressure. *J Biomater Tissue Eng*. 2014;**4**(9):749-54. DOI: http://dx.doi.org/10.1166/jbt.2014.1221.
30. Abdi M, Karimi A, Navidbakhsh M, Hassani K, Faghihi S. Modeling of cerebral aneurysm using equivalent electrical circuit (Lumped Model). *Perfusion*. 2014;**29**(2):142-52. doi: 10.1177/0267659113498617. PubMed PMID: 23887086.
31. Abdi M, Karimi A, Navidbakhsh M, Pirzad Jahromi G, Hassani K. A lumped parameter mathematical model to analyze the effects of tachycardia and bradycardia on the cardiovascular system. *Int J Numer Model*. 2014;**27**:[1 p.]. doi: 10.1002/jnm.2010.
32. Barati E, Halabian M, Karimi A, Navidbakhsh M. Numerical Evaluation of Stenosis Location Effects on Hemodynamics and Shear Stress Through Curved Artery. *J Biomater Tissue Eng*. 2014;**4**(5):358-66. DOI: http://dx.doi.org/10.1166/jbt.2014.1176.
33. Deatsch AE, Evans BA. Heating efficiency in magnetic nanoparticle hyperthermia. *J Magn Magn Mater*. 2014;**354**:163-72. doi: http://dx.doi.org/10.1016/j.jmmm.2013.11.006.
34. Stauffer PR, Diederich CJ, Seegenschmiedt MH. Interstitial heating technologies. In: Seegenschmiedt MH, Fessenden P, Vernon CC, editors. Thermoradiotherapy and thermochemotherapy. Berlin, Heidelberg: Springer; 1995. p. 279-320. Doi: 10.1007/978-3-642-57858-8_13.
35. Nedelcu G. Magnetic nanoparticles impact on tumoral cells in the treatment by magnetic fluid hyperthermia. *Dig J Nanomater Biostruct*. 2008;**3**(3):103-7.
36. Rosensweig RE. Heating magnetic fluid with alternating magnetic field. *J Magn Magn Mater*. 2002;**252**:370-4. doi: http://dx.doi.org/10.1016/S0304-8853(02)00706-0.
37. Jain RK. Transport of molecules, particles, and cells in solid tumors. *Annu Rev Biomed Eng*. 1999;**1**:241-63. doi: 10.1146/annurev.bioeng.1.1.241. PubMed PMID: 11701489.